Type-I intermittency with discontinuous reinjection probability density in a truncation model of the derivative nonlinear Schrödinger equation

Gustavo Krause · Sergio Elaskar · Ezequiel del Río

Abstract In previous papers, the type-I intermittent phenomenon with continuous reinjection probability density (RPD) has been extensively studied. However, in this paper type-I intermittency considering discontinuous RPD function in one-dimensional maps is analyzed. To carry out the present study the analytic approximation presented by del Río and Elaskar (Int. J. Bifurc. Chaos 20:1185–1191, 2010) and Elaskar et al. (Physica A. 390:2759–2768, 2011) is extended to consider discontinuous RPD functions. The results of this analysis show that the characteristic relation only depends on the position of the lower bound of reinjection (LBR), therefore for the LBR below the tangent point the relation $\langle l \rangle \propto \varepsilon^{-1/2}$, where ε is the control parameter, remains robust regardless the form of the RPD, although the average of the laminar phases $\langle l \rangle$ can change. Finally, the study of discontinuous RPD for type-I intermittency which occurs in a three-wave truncation model for the derivative nonlinear Schrodinger equation is presented. In all tests the theoretical results properly verify the numerical data.

Keywords Intermittency · Discontinuous reinjection probability density · Characteristic relation · DNLS equation

1 Introduction

Intermittency is a particular route to deterministic chaos, where a transition between regular or laminar and chaotic phases occurs. The concept of intermittency was introduced by Pomeau and Manneville [1,2]. In the intermittency phenomenon, when a control parameter exceeds a threshold value, the system behavior changes abruptly to a larger attractor by means of an explosive bifurcation [3]. This phenomenon has been observed in several physical topics such as Lorenz system, Rayleigh-Bénard convection, forced nonlinear oscillators, plasma physics, turbulence, porous media, combustion, reaction diffusion systems, etc. [4–11]. Some examples of control parameters for these physical systems are the Rayleigh number, the excitation frequency, the damping coefficient, etc. On the other hand, this phenomenon has been found in subjects of economical and medical sciences [12–14]. Traditionally, intermittency has been classified into three different types called I, II, and III [3,15] according to the Floquet multipliers or eigenvalues in the local Poincaré map. Subsequent studies extended the classification to type X, V, and on-off intermittencies [16–18]. To generate intermittency, it is necessary to have a reinjection mechanism that maps back from the chaotic zone into

the local regular or laminar one. This mechanism is described by the reinjection probability density function (RPD), which is defined by the nonlinear dynamics of the system itself.

To characterize the intermittency phenomenon it is necessary to determine the statistical properties of the reinjection processes such as the probability density of the laminar phases, the average of the laminar phases, and the characteristic relation $\langle l \rangle \propto \varepsilon^{-\beta}$ that relates the average of the laminar phases $\langle l \rangle$ to the control parameter ε through the critical exponent β. In order to do this, it is necessary to know the RPD. Therefore, the accurate evaluation of this function is extremely important to correctly analyze and describe the intermittency phenomenon. However, only in a few cases it is possible to obtain an analytical expression for the RPD. Also, it is not a simple task to experimentally or numerically obtain the RPD due to the huge amount of data needed. Besides this, the statistical fluctuations induced in the numerical computations and the experimental measurements are difficult to estimate. For these reasons several different approaches have been used to describe the RPD in intermittent systems. The most popular approach is to consider the RPD as a constant, i.e., to assume a uniform reinjection [4,5,19,20], which is not suitable for many problems. Also, different approaches have been implemented using a characteristic of the particular nonlinear processes, but these RPD functions cannot be applied for other systems. Recently a more general estimate of the RPD has been introduced [22,23], which includes the uniform reinjection as a particular case.

In the particular case of type-I intermittency, studies have been performed considering uniform [21] or monotonically decreasing RPD functions [20]. However, these RPD have been considered in maps where the lower boundary of reinjection (LBR), which indicates the minimum value that can be reached by the returning orbits, is placed within the laminar interval. When the LBR point is positioned away from the lower end of the laminar interval, the RPD is discontinuous because the position of the LBR produces a reinjection concentration at the beginning of the laminar region, due to the orbits that return below the lower bound of the laminar interval can only be reinjected in that region (for more details see the next section).

In this paper the statistical properties of type-I intermittency with discontinuous RPD function are analyzed. The local maps studied are quadratic where the return mechanisms are produced by a function $g(x) \propto x^{\gamma}$. This function allows to model different functions RPD for different exponents γ. To evaluate the statistical properties, the methodology developed in [22–25] is adapted to capture discontinuous RPD. The results obtained in this analysis extend the conclusions of previous studies [20], showing that the characteristic relation only depends on the LBR position regardless of the RPD form. In this way, when the LBR is far below the lower bound of the laminar region, although the RPD becomes discontinuous due to the concentration of reinjection points at the beginning of the laminar interval with the consequent increase in the average laminar length, the relation $\langle l \rangle \propto \varepsilon^{-1/2}$ remains unchanged. Finally, the extended methodology is used to calculate the discontinuous RPD in a physical example: the three-wave truncation model of the derivative nonlinear Schrödinger equation (DNLS). The theoretical results show very good accuracy with respect to numerical data.

2 Map description

In this paper, for type-I intermittency study a widely used map is considered to represent the local map

$$x_{n+1} = f(x) = a\,x_n^2 + x_n + \varepsilon, \tag{1}$$

where ε is the control parameter. For $\varepsilon < 0$ there are two fixed points, one stable and the other unstable which collapse on one fixed point $x_0 = 0$ for $\varepsilon = 0$. This fixed point disappears for $\varepsilon > 0$, and a laminar channel between the map and the bisector line emerges, whose width is defined by the control parameter ε, since it specifies the distance between the local Poincaré map and the bisector line. The parameter $a > 0$ specifies the position of the function's minimum (point with zero-derivative).

By the definition of the map, the function's minimum coincides with the lower bound of reinjection, x_{LBR}, that is:

$$\left.\frac{\mathrm{d}f}{\mathrm{d}x}\right|_{x_{\mathrm{LBR}}} = 0, \tag{2}$$

hence

$$x_{\mathrm{LBR}} = -\frac{1}{2a}. \tag{3}$$

However, it is not essential for the validity of the method that is presented in this work, as shown in

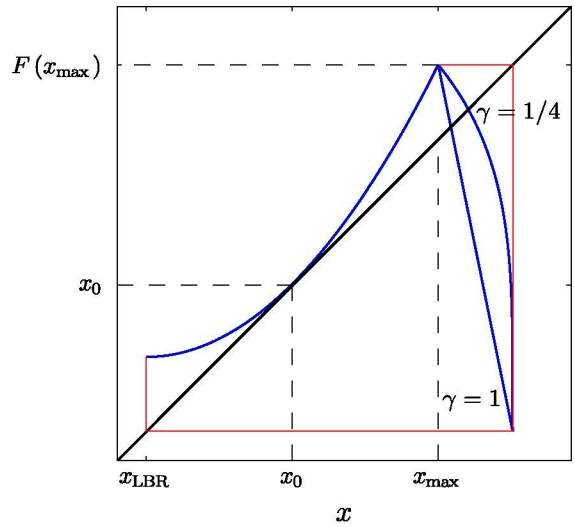

Fig. 1 $F(x)$ map given by Eq. (6) for $\gamma = 1$ and $\gamma = 1/4$ with the bisector line and $\varepsilon = 0$

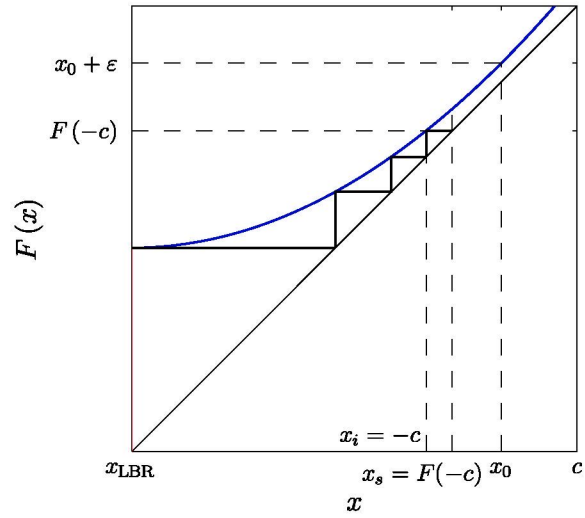

Fig. 2 Trajectory starting at the point LBR for $\varepsilon > 0$. Arrangement of points $x_i = -c$ and $x_s = F(-c)$

Sect. 5, where the LBR does not coincide with the local minimum of the map.

In order that the intermittency phenomenon occurs, as well as the Poincaré local map a reinjection mechanism that returns the trajectories from the chaotic phase to the laminar one is necessary. Here, a reinjection mechanism is implemented by the following general function (Fig. 1):

$$g(x) = x_{\mathrm{LBR}} + h\,[f(x_{\max}) - x]^{\gamma}\,, \quad \gamma > 0, \tag{4}$$

where $x_{\max}$ is the intersection point between the local map, Eq. (1), and the reinjection map, Eq. (4). The coefficient h is given by $g(x_{\max}) = f(x_{\max})$, thus

$$h = \frac{f(x_{\max}) - x_{\mathrm{LBR}}}{[f(x_{\max}) - x_{\max}]^{\gamma}}. \tag{5}$$

Equation (4) permits to analyze different reinjection processes as the exponent γ changes. Then, the complete map $F(x)$ is defined by:

$$F(x) = \begin{cases} f(x) = a\,x^2 + x + \varepsilon, & x \le x_{\max} \\ g(x) = x_{\mathrm{LBR}} + h\,[f(x_{\max}) - x]^{\gamma} & x > x_{\max}, \end{cases} \tag{6}$$

where the cases of interest are given for $\varepsilon > 0$ and $a > 0$.

This map has two different reinjection mechanisms, one of them is given directly by the function $g(x)$ and the other one is produced by trajectories passing through points $x < -c$, where c is the tolerance set for the laminar phases which has to be small in order to permit the use of the differential approximation of Eq. (16) within the laminar interval $[-c, c]$. As a consequence of these different reinjections, the RPD will present a discontinuous form, since, while $g(x)$ reinjects points in the whole laminar interval, the reinjected points x_j with $F^{-1}(x_j) < -c$ will be reinjected only inside of the sub-laminar interval $[-c, F(-c))$, since all these points satisfy $F(x_j) < F(-c)$. Consequently, a discontinuity in the RPD appears at point $x_s = F(-c)$. It should be noted that for the calculation of the RPD only the position of the first iteration within the laminar region is necessary, regardless the subsequent evolution.

Kim et al. [20] partially studied this phenomenon however, they did not analyze the complex RPD structure inside the $[-c, F(-c))$ sub-interval, considering only continuous and monotonically decreasing RPD. This paper studies the more complex form of the RPD, showing that the characteristic relation $\langle l \rangle \sim \varepsilon^{-\beta}$ holds also for discontinuous and not necessarily decreasing RPD.

For points reinjected directly from the function $g(x)$ the exponent γ determines the RPD function form [22,23]. If $\gamma = 1$ the RPD is approximately uniform because $g(x)$ is linear. If $0 < \gamma < 1$, the map verifies $\mathrm{d}g(x)/\mathrm{d}x|_{f(x_{\max})} \to \infty$, and the trajectories spend a

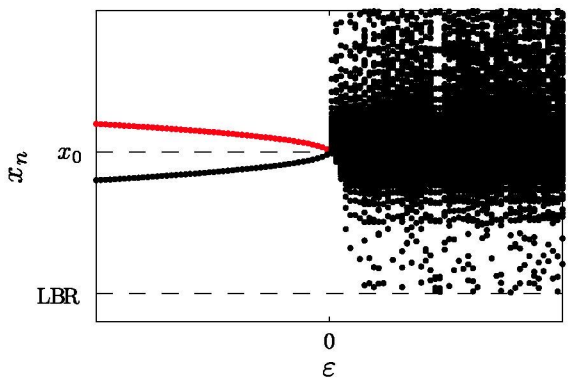

Fig. 3 Bifurcation diagram for Eq. (6) with $\gamma = 1$

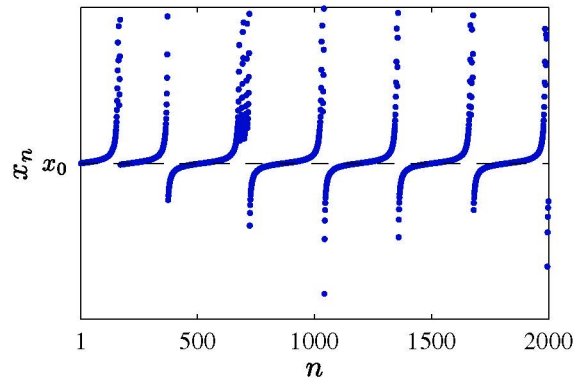

Fig. 4 Laminar and chaotic phases for $\varepsilon = 10^{-3}$, $a = 1$, $\gamma = 1$, and $c = 10^{-2}$

lot of time in the upper region of the map. In these cases the RPDs in the sub-interval $[F(-c), c]$ are monotonically increasing functions. For $\gamma > 1$, the map verifies $\mathrm{d}g(x)/\mathrm{d}x|_{f(x_{\max})} = 0$ and the trajectories evolve very close to the LBR point where the derivative is also zero.

The map (Eq. 6) is shown in Fig. 1 for two different values of the parameter γ. Note that as the derivative is zero at the point LBR, the reinjection point of the orbit passing at x_{LBR} can be a critical point where the RPD $\to \infty$ [22]. In order to simplify the expressions by ensuring that the critical reinjection is produced at the left end of the laminar interval $(-c)$, without loss of generality this point is fixed to a point x_i which corresponds to the first iteration of the zero-derivative trajectory that satisfies the tolerance set for the laminar region. Therefore, the semi-longitude is redefined as $-c = x_i$ (Fig. 2). The next iteration of x_i defines the sub-interval $[x_i, x_s)$, where $x_s = F(x_i) = F(-c)$, within which all trajectories passing through $x < -c$ will be reinjected, generating the concentration of reinjection points that will produce the discontinuity of the RPD at point x_s.

In Fig. 3 the bifurcation diagram for map (Eq. 6) is illustrated: for $\varepsilon < 0$ there are two fixed points, and for $\varepsilon > 0$ there is chaos. Figure 4 indicates the time-iteration evolution showing the characteristic alternation of the laminar and chaotic phases for type-I intermittency.

Results for $\gamma > 1$ do not possess relevance in this research because $\mathrm{d}g(x)/\mathrm{d}x|_{f(x_{\max})} = 0$. Then there is a high concentration of trajectories around $x = F(x_{\max})$. The trajectories starting around $x = F(x_{\max})$ are mapped close to the LBR point producing a high value of the RPD in the lower bound of the laminar interval $x = -c$. In this case the RPD tends towards a delta-function.

3 Analytic approximation for the RPD function

The previous section explained that the RPD could be a discontinuous function. Therefore, to obtain the analytical formulation for the RPD, $\phi(x)$, it is considered that it can be composed of two continuous functions $\phi_1(x)$ and $\phi_2(x)$. The first function is defined in the sub-interval $[x_i, x_s]$ to model the reinjections of trajectories evolving through $x < -c$. The second one is applied to the remaining part of the laminar interval, that is $[x_s, c]$, to model the reinjections coming from function $g(x)$.

It should be noted that although the reinjections of $g(x)$ can fall in the whole laminar interval $[-c, c]$, $\phi_2(x)$ is not applied in the sub-interval $[x_i, x_s]$. This is because the influence of the reinjections due to $g(x)$ can be neglected with respect to the reinjection points x_j with $F^{-1}(x_j) < -c$. Therefore, it can be thought that each region has a different reinjection mechanism. This assumption allows to considerably simplify the expressions.

To obtain $\phi_1(x)$ and $\phi_2(x)$, the methodology presented in [22–25] is used, because in each sub-interval the associated functions $M(x)$ have approximately linear forms.

In the cited works the function RPD is evaluated using an auxiliary function $M(x)$ which is obtained from numerical or experimental data and is defined as:

$$M(x) = \frac{\int_{x_i} \tau\, \phi(\tau)\, \mathrm{d}\tau}{\int_{x_i}^{x} \phi(\tau)\, \mathrm{d}\tau}. \tag{7}$$

The integral $M(x)$ smooths the experimental or numerical data series, and its numerical estimation is more robust than the direct evaluation of the function $\phi(x)$. As the function $M(x)$ is an average over the reinjection points in the laminar interval, its evaluation is easier than the direct RPD calculation:

$$M(x_q) = \frac{1}{q} \sum_{j=1}^{q} x_j, \tag{8}$$

where the reinjection points $\{x_j\}_{j=1}^{N}$ must be sorted from lowest to highest, i.e., $x_j \leq x_{j+1}$.

The method based on the function $M(x)$ has been tested in a wide class of maps exhibiting intermittency: in type-I [25], type-II [22], and type-III [23] intermittencies, in type-II and III with presence of noise [24], in classical pathological cases [26]. In all cases $M(x)$ satisfy a linear approximation:

$$M(x) = m\,(x - x_i) + x_i, \tag{9}$$

where x_i is the lowest reinjection point.

Using the definition (Eq. 7) and the approximation of Eq. (9), the RPD, $\phi(x)$, can be written as [23]:

$$\phi(x) = b\,(x - x_i)^{\alpha}, \quad \text{with} \quad \alpha = \frac{2m-1}{1-m}, \tag{10}$$

where b is a normalization parameter which is obtained by the condition $\int \phi(x)\, \mathrm{d}x = 1$.

Having into account that in each region where functions $\phi_1(x)$ and $\phi_2(x)$ are defined, the associated functions $M(x)$ present a linear form, according to the previous results it is proposed:

$$\phi(x) = \begin{cases} \phi_1(x) = b\,(x - x_i)^{\alpha_1}, & x < x_s, \\ \phi_2(x) = bk\,(x - x_i)^{\alpha_2}, & x \geq x_s, \end{cases} \tag{11}$$

where the exponents α_1 and α_2 are obtained from:

$$\alpha_{1,2} = \frac{2m_{1,2} - 1}{1 - m_{1,2}}, \tag{12}$$

being m_1 the slope of function $M_1(x) = m_1\,(x - x_i) + x_i$ defined in $[x_i, x_s]$ and m_2 the slope of $M_2(x) = m_2\,(x - x_s) + x_s$ calculated with points $x > x_s$.

The factor k in Eq. (11) is used to evaluate the different number of reinjections from region $x < -c$ with respect to trajectories coming from $g(x)$. This parameter is obtained by means of the definition of $M(x)$, as explained below.

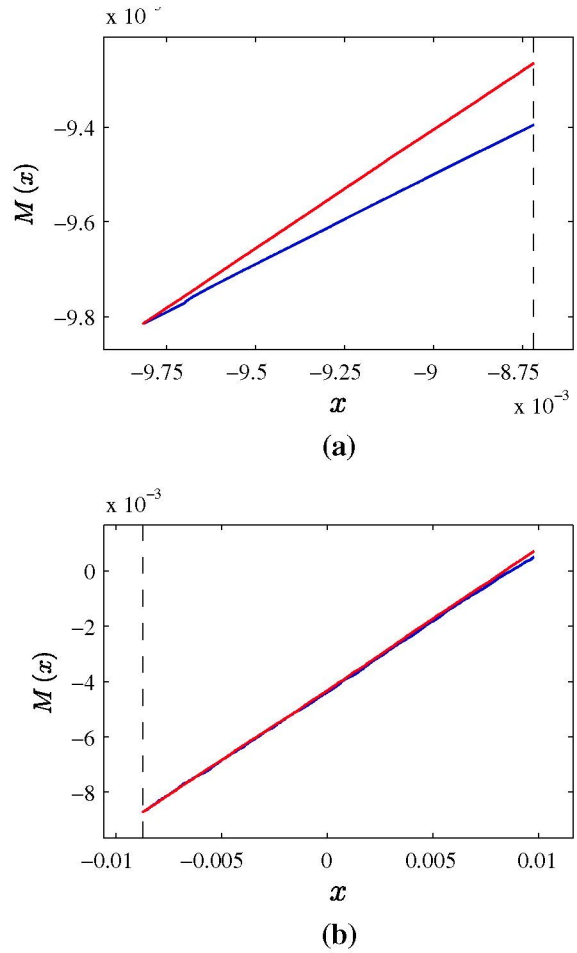

Fig. 5 **a** Function $M(x)$ for $\varepsilon = 10^{-3}$, $c = 10^{-2}$, $\gamma = 1$ (*blue lines*) and $\gamma = 1/4$ (*red lines*). **a** Sub-interval $[x_i, x_s)$: $m_{\gamma=1} = 0.386$, $m_{\gamma=1/4} = 0.502$. **b** Sub-interval $[x_s, c]$: $m_{\gamma=1} = 0.504$, $m_{\gamma=1/4} = 0.519$. In all cases $M(x)$ is approximately linear. (Color figure online)

It should be noted that the point x_i is a singular point of $\phi(x)$ where the function $\phi_1(x)$ satisfies $\phi_1(x_i) \to \infty$ if $\alpha_1 < 0$ and $\phi_1(x_i) \to 0$ if $\alpha_1 > 0$.

In Fig. 5 two different results for functions $M_1(x)$ and $M_2(x)$ are shown. It can be observed the linear form of both functions. Similar behaviors are obtained independently on the initial parameters ε, a, and γ.

Figure 5b shows that $m_{\gamma=1} \approx m_{\gamma=1/4} \approx 1/2$. The result $m = 1/2$ is the specific case of uniform reinjection. Since the laminar interval $[-c, c]$ is small, $g(x)$ behaves as a linear function and consequently $m_2 \approx 1/2$ even for $\gamma = 1/4$.

$$M(x) = \frac{\int_{x_i}^{x_s} \tau\, \phi_1(\tau)\, \mathrm{d}\tau + \int_{x_s}^{x} \tau\, \phi_2(\tau)\, \mathrm{d}\tau}{\int_{x_i}^{x_s} \phi_1(\tau)\, \mathrm{d}\tau + \int_{x_s}^{x} \phi_2(\tau)\, \mathrm{d}\tau}$$

$$= \frac{(x_s - x_i)^{\alpha_1+1}\, \frac{x_s(\alpha_1+1)+x_i}{(\alpha+1)(\alpha_1+2)} + k\,(x - x_i)^{\alpha_2+1}\, \frac{x(\alpha_2+1)+x_i}{(\alpha_2+1)(\alpha_2+2)} - k\,(x_s - x_i)^{\alpha_2+1}\, \frac{x(\alpha_2+1)+x_i}{(\alpha_2+1)(\alpha_2+2)}}{\frac{(x_s-x_i)^{\alpha_1+1}}{(\alpha_1+1)} + k\frac{(x-x_i)^{\alpha_2+1}}{(\alpha_2+1)} - k\frac{(x_s-x_i)^{\alpha_2+1}}{(\alpha_2+1)}} \tag{13}$$

$$k = \frac{(x_s - x_i)^{\alpha_1+1}\, \frac{x_s(\alpha_1+1)+x_i}{(\alpha+1)(\alpha_1+2)} - \frac{M(x)}{(\alpha_1+1)}\,(x_s - x_i)^{\alpha_1+1}}{\frac{M(x)}{(\alpha_2+1)}\left[(x - x_i)^{\alpha_2+1} - (x_s - x_i)^{\alpha_2+1}\right] - \frac{(x-x_i)^{\alpha_2+1}[x(\alpha_2+1)+x_i]-(x_s-x_i)^{\alpha_2+1}[x_s(\alpha_2+1)+x_i]}{(\alpha_2+1)(\alpha_2+2)}} \tag{14}$$

$$b = \left\{ \frac{1}{\alpha_1 + 1}\,(x_s - x_i)^{\alpha_1+1} + \frac{k}{\alpha_2 + 1}\left[(c - x_i)^{\alpha_2+1} - (x_s - x_i)^{\alpha_2+1}\right] \right\}^{-1}. \tag{15}$$

Since the exponents α_1 and α_2 are known, and due to the global function $M(x)$ does not depend on the parameter b, it remains only the factor k, hence it can be evaluated. By means of the definition given in Eq. (7) the function $M(x)$ for $x > x_s$ is shown in Eq. (13). Note that for points $x < x_s$ the function $M(x)$ is linear, however for $x > x_s$ the function $M(x)$ has a nonlinear form.

If the function $M(x)$ is evaluated at some point $x > x_s$, it is possible to explicitly obtain the factor k, which is expressed in Eq. (14). Finally, using the normalization condition the parameter b is shown in Eq. (15).

Figure 6 shows the functions $M(x)$ and the RPD $\phi(x)$ for two values of ε and γ. The numerical data are indicated in blue and the red lines represent the theoretical results which show a very good accuracy.

4 Characteristic relations

Following [15], the laminar length can be calculated using a continuous approximation for the local Poincaré map given by Eq. (1):

$$\frac{\mathrm{d}x}{\mathrm{d}l} = ax^2 + \varepsilon, \tag{16}$$

where l indicates the number of iterations inside of the laminar interval and the control parameter ε is assumed to be small. By integration the above equation results:

$$l(x, c) = \frac{1}{\sqrt{a\varepsilon}}\left[\tan^{-1}\left(\sqrt{\frac{a}{\varepsilon}}c\right) - \tan^{-1}\left(\sqrt{\frac{a}{\varepsilon}}x\right)\right]. \tag{17}$$

The laminar length does not depend on the reinjection mechanism, however it depends only on the local Poincaré map. Note that the last expression is valid for $\varepsilon \to 0$.

The average laminar length $\langle l \rangle$ depends on the local map by means of the laminar length $l(x, c)$ and on the reinjection mechanism through the RPD function $\phi(x)$:

$$\langle l \rangle = \int_{-c}^{c} \phi(x)\, l(x, c)\, \mathrm{d}x. \tag{18}$$

Taking into consideration Eq. (11), the last expression can be written as:

$$\langle l \rangle = \int_{-c}^{x_s} \phi_1(x)\, l(x, c)\, \mathrm{d}x + \int_{x_s}^{c} \phi_2(x)\, l(x, c)\, \mathrm{d}x. \tag{19}$$

The solution of the first term is reduced to solve only the integral of $\phi_1(x)$, because in the sub-interval $[x_i, x_s)$ the laminar length verifies $l(x, c) = l(-c, c)$, since all trajectories starting at that sub-interval spend the same number of iterations to leave the laminar region. Then the last expression can be written as:

$$\langle l \rangle = l(-c, c)\frac{b\,(x_s - x_i)^{\alpha_1+1}}{\alpha_1 + 1} + \int_{x_s}^{c} \phi_2(x)\, l(x, c)\, \mathrm{d}x. \tag{20}$$

The second integral in Eq. (19) does not have an analytical solution, therefore it must be solved numerically. Taking into account that $\phi_2(x)$ and $l(x, c)$ are continuous functions, by applying the mean value theorem there is a value x' in (x_s, c) such that

$$\int_{x_s}^{c} \phi_2(x)\, l(x, c)\, \mathrm{d}x = (c - x_s)\phi_2(x')\, l(x', c). \tag{21}$$

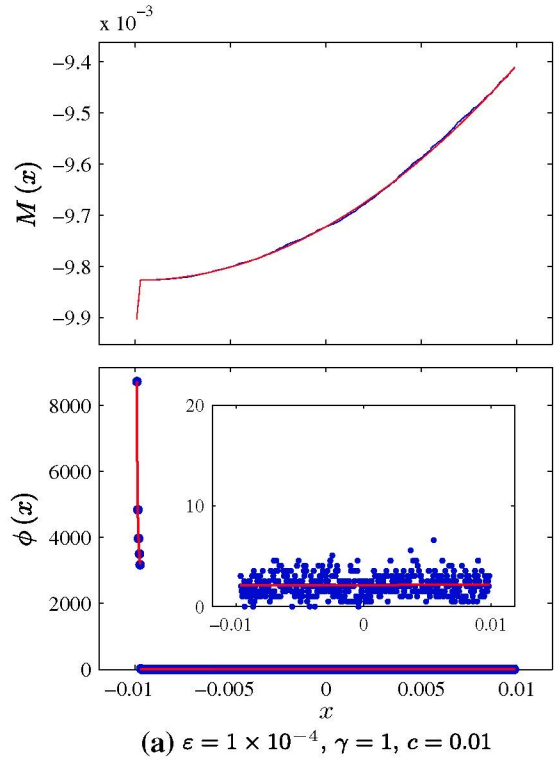

(a) $\varepsilon = 1 \times 10^{-4}$, $\gamma = 1$, $c = 0.01$

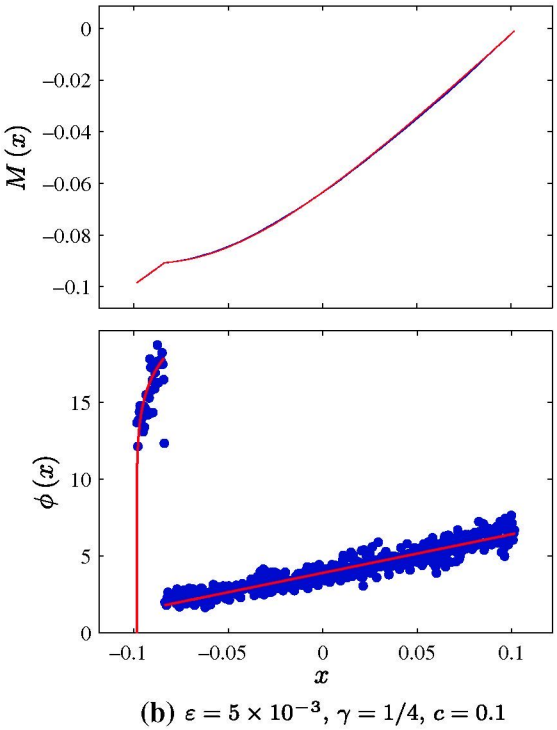

(b) $\varepsilon = 5 \times 10^{-3}$, $\gamma = 1/4$, $c = 0.1$

Fig. 6 Functions $M(x)$ and $\phi(x)$ for $a = 1$ and considering two different values for ε, γ and c

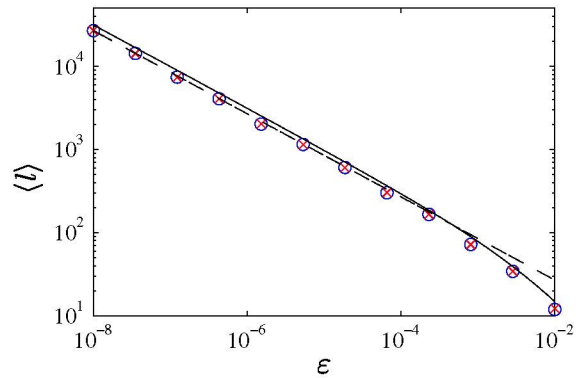

(a) $\gamma = 1$

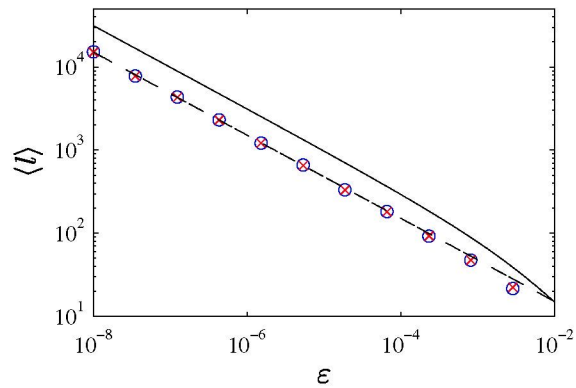

(b) $\gamma = 1/4$

Fig. 7 Average laminar length versus the control parameter for $c = 0.10$. The *red crosses* show theoretical results, and the *blue circles* indicate numerical data (both results are very similar). The *continuous line* represents the maximum laminar length $l(-c, c)$. (Color figure online)

Note that $\phi_2(x')$ is a finite non-zero value in the interval $(\phi_{2\min}, \phi_{2\max})$ where $\phi_{2\min}$ and $\phi_{2\max}$ refer to the minimum and maximum values of $\phi_2(x)$ with x in (x_s, c), hence the limit of Eq. (21) when ε goes to zero is proportional to the corresponding limit of $l(x', c)$.

By means of Eqs. (17), (20), and (21), the average laminar length when ε goes to zero is $\langle l \rangle \propto \varepsilon^{-1/2}$.

Figure 7 shows $\langle l \rangle$ as a function of the control parameter ε. Numerical data is plotted in blue circles and the theoretical results in red crosses. The continuous line indicates the maximum laminar length in order to visualize the influence of the RPD form. Figure 7b shows that for an increasing RPD (Fig. 6b) the average laminar length goes apart from the maximum value $l(-c, c)$. On the contrary, a decreasing RPD produces $\langle l \rangle \to l(-c, c)$. The dashed line shows the characteristic relation for type-I intermittency $\langle l \rangle \propto \varepsilon^{-1/2}$.

The numerical data are plotted in blue and the theoretical results in red. The continuous lines indicate the maximum laminar lengths $l_{\max} = l(-c, c)$ and the dotted lines show the characteristic relation for type-I intermittency: $\langle l \rangle \propto \varepsilon^{-1/2}$.

Note that the characteristic relation for type-I intermittency is $\langle l \rangle \sim \varepsilon^{-\beta}$ (for $\varepsilon \to 0$), where β is a constant. From the figure, it is possible to observe that $\beta = 1/2$ is verified in both cases independently of the RPD shape. Therefore, the RPD function does not need to be continuous, or monotonically decreasing to satisfy the characteristic relation with $\beta = -1/2$.

The probability density of the laminar lengths, $\phi_l(l)$, is determined following [15]:

$$\phi_l(l) = \phi[X(l, c)] \left| \frac{\mathrm{d}X(l, c)}{\mathrm{d}l} \right|, \tag{22}$$

where $X(l, c)$ is the inverse of $l(x, c)$ given by Eq. (17)

$$X(l, c) = \sqrt{\frac{\varepsilon}{a}} \tan \left[\tan^{-1} \left(\sqrt{\frac{a}{\varepsilon}} c \right) - \sqrt{a\varepsilon}\, l \right]. \tag{23}$$

Figure 8 shows the numerical data and analytical results for the probability density of the laminar length, $\phi_l(l)$. In the same way as the previous figures, blue color indicates the numerical data and red lines represent the theoretical approach. It is possible to observe the good accuracy between the analytical and numerical results.

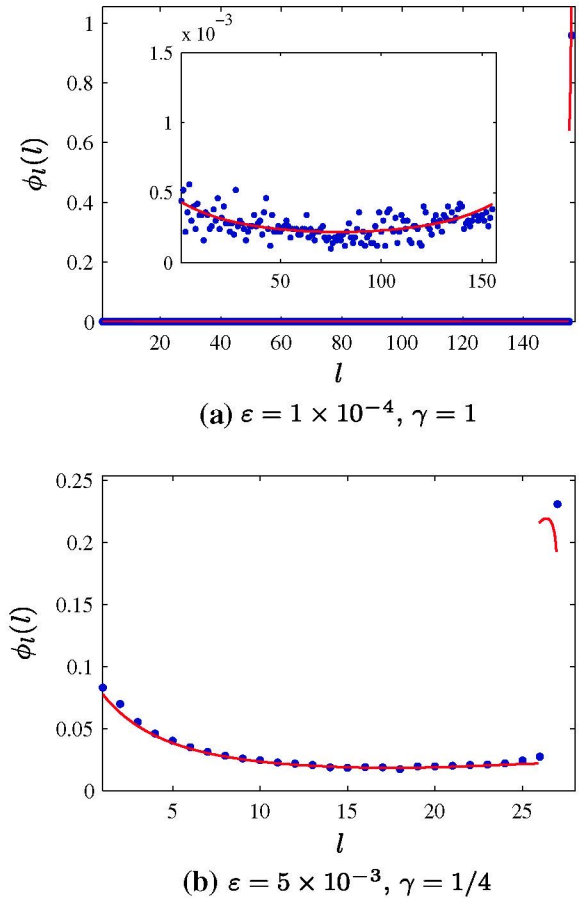

Fig. 8 Probability of the laminar length for map (Eq. 6) for the values used in Fig. 6

5 Intermittency in the DNLS equation

A physical example showing type-I intermittency with discontinuous RPD can be found in the three-wave truncation model of the DNLS.

The DNLS equation describes the evolution of circularly polarized Alfvén waves of finite amplitude propagating parallel or near-parallel to an unperturbed uniform magnetic field in a cold, homogeneous plasma, using a two-fluid, quasi-neutral approximation with electron inertia and current displacement neglected. Taking the unperturbed magnetic field B_0 in the z direction, the DNLS equation reads [27–29]:

$$\frac{\partial B}{\partial t} + \frac{\partial}{\partial z}\left(|B|^2 B\right) + \mathrm{i}\frac{\partial^2 B}{\partial z^2} + \hat{\gamma} B = 0, \tag{24}$$

where the positive sign in the dispersive term corresponds to a left-hand circularly polarized wave propagating in the z direction, $\hat{\gamma}$ is an appropriate damping/driving linear operator, and the dimensionless variables B, z, t are defined by [7]:

$$B = \frac{B_x + B_y}{2B_0}, \quad 2\Omega_{\mathrm{i}} t \to t, \quad \frac{2\Omega_{\mathrm{i}}}{V_{\mathrm{A}}} z \to z, \tag{25}$$

being B_0 the reference magnetic field module, Ω_{i} the ionic cyclotron frequency and V_{A} the Alfvén velocity.

A three-wave truncation model allows to obtain an approximated solution which consists of three traveling waves satisfying the resonance condition $2k_0 = k_1 + k_2$:

$$B(z, t) = \sum_{j=0}^{2} a_j \exp\left[\mathrm{i}\left(k_j z - \omega_j t + \psi_j\right)\right], \tag{26}$$

where $a_j(t)$ and $\psi_j(t)$ are real numbers. Wave number and frequency of modes are related by the lossless dis-

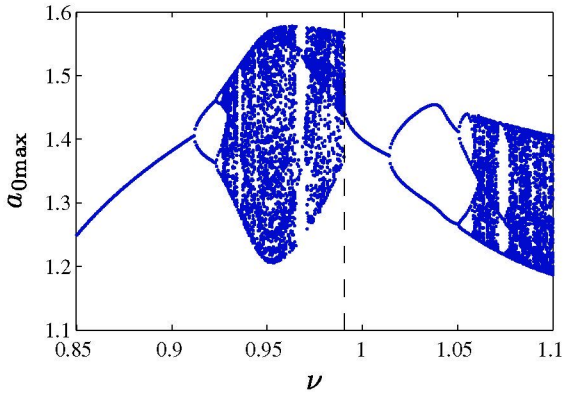

Fig. 9 Bifurcation diagram for the three-wave truncation model of the DNLS equation

persion relation for circularly polarized Alfvén waves at low wave number $\omega_j = \mp k_j^2$. Considering that the non-resonant modes are damped for $t \to \infty$, the amplitudes a_j can be determined [7].

Type-I intermittency appears if the k_0 wave is linearly excited and the other two waves have linear Landau damping $\hat{\gamma} = -\eta\, \partial/\partial z \propto \nu$, where ν is a relationship between resonant wave numbers and the system damping [7].

Figure 9 shows the maximum amplitude evolution of the k_0 wave versus the control parameter ν. The figure shows a complex dynamic behavior including fixed points, bifurcations, and chaotic behavior. A periodic orbit loses its stability close to $\nu \approx 0.99$ generating type-I intermittency for $\nu \lesssim 0.99$.

To analyze the intermittency a Poincaré map is constructed using the numerical data of the three-wave truncation model for $\nu \approx 0.99$. The map is illustrated in Fig. 10. Note that the map has a tangent point at $a_{0\max} \approx 1.45$ and two points with zero-derivatives, where $a_{0\,\max}$ represents the maximum amplitude of the mother wave. These points have a strong influence in the reinjection process. Also, the LBR is away from the tangent point. Therefore, the RPD function will be discontinuous and it will have two singular points where $\phi(x) \to \infty$.

The numerical data $a_{0\max n}$, $a_{0\max n+1}$ are used to construct the Poincaré map. The channel width between the function and the bisector line is defined by $a_{0\max n+1} + \varepsilon$, where ε is used as the control parameter instead of ν.

Due to the presence of the zero-derivatives, the reinjection process for this map produces two singular

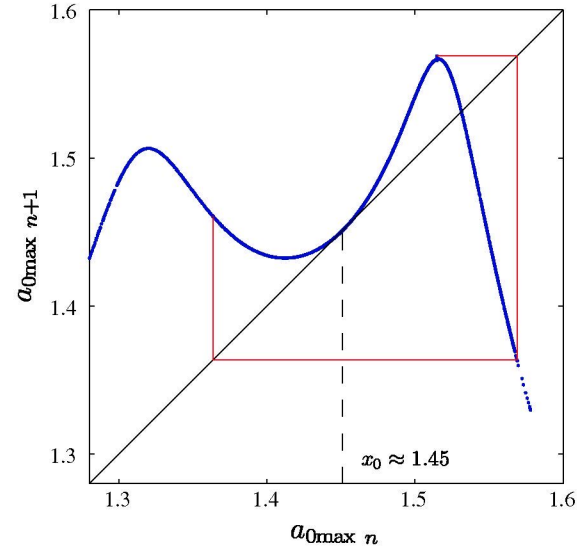

Fig. 10 Map for $\nu \approx 0.985$

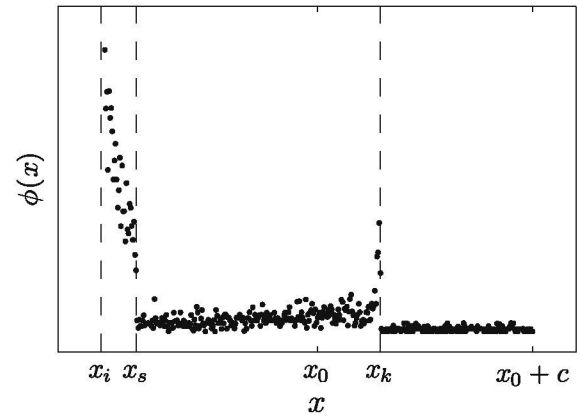

Fig. 11 Function RPD for the map of Fig. 10. x_i and x_k are critical points, where $|\mathrm{d}\phi/\mathrm{d}x| \to \infty$ and the jump occurs at $x_s = F(x_i)$

points where the RPD tends to infinity ($\phi(x) \to \infty$). One of them corresponds to the reinjection of to the trajectory passing through the local minimum point, defining the lower bound of the laminar region, $x_i = x_0 - c$, in the same way as the previous analysis. On the other hand, the trajectory passing through the zero-derivative corresponding to the maximum of the map determines the other singular point, x_k. The upper bound of the laminar interval is defined by $x_0 + c$. In Fig. 11 is plotted a typical RPD for the truncated DNLS equation, where the critical points are shown.

From Fig. 11, it is proposed the following function for modeling the RPD:

$$\phi(x) = \begin{cases} \phi_1(x) = b\,(x - x_i)^{\alpha_1}\,, & x < x_s, \\ \phi_2(x) = bk_2\,(x_k - x)^{\alpha_2}\,, & x_s \le x < x_k, \\ \phi_3(x) = bk_3\,(x - x_i)^{\alpha_3}\,, & x \ge x_k, \end{cases} \tag{27}$$

where the factors k_2 and k_3 are again evaluated using the function $M(x)$. Note that the RPD corresponding to function $M(x)$. To calculate the exponent α_2, points inside the interval $x_s \le x < x_k$ are used. However, one has to take into consideration that $\phi_2(x) \to \infty$ for the right extreme of the interval, therefore, the function $M(x)$ is calculated from x_k to x_s using the auxiliary points $x'_j = x_k + (x_k - x_j)$. Finally, the reinjection points $x_j \ge x_k$ are used to calculate the exponent α_3.

$$M(x) = \begin{cases} M_1(x) = \dfrac{x\,(1+\alpha_1) + x_i}{\alpha_1 + 2}, & x < x_s, \\ M_2(x) = \dfrac{\begin{array}{r}(x_s - x_i)^{\alpha_1+1}\,\dfrac{x_s\,(\alpha_1+1) + x_i}{(\alpha_1+1)\,(\alpha_1+2)} + \\ -k_2 \dfrac{(x_k - x)^{\alpha_2+1}\,[x\,(\alpha_2+1) + x_k] - (x_k - x_s)^{\alpha_2+1}\,[x_s\,(\alpha_2+1) + x_k]}{(\alpha_2+1)\,(\alpha_2+2)}\end{array}}{\dfrac{(x_s - x_i)^{\alpha_1+1}}{\alpha_1+1} - k_2 \dfrac{(x_k - x)^{\alpha_2+1} - (x_k - x_s)^{\alpha_2+1}}{\alpha_2+1}}, & x_s \le x < x_k, \\ M_3(x) = \dfrac{\begin{array}{r}(x_s - x_i)^{\alpha_1+1}\,\dfrac{x_s\,(\alpha_1+1) + x_i}{(\alpha_1+1)\,(\alpha_1+2)} + k_2\,(x_k - x_s)^{\alpha_2+1}\,\dfrac{x_s\,(\alpha_2+1) + x_k}{(\alpha_2+1)\,(\alpha_2+2)} + \\ k_3 \dfrac{(x - x_i)^{\alpha_3+1}\,[x\,(\alpha_3+1) + x_i] - (x_k - x_i)^{\alpha_3+1}\,[x_k\,(\alpha_3+1) + x_i]}{(\alpha_3+1)\,(\alpha_3+2)}\end{array}}{\dfrac{(x_s - x_i)^{\alpha_1+1}}{\alpha_1+1} + k_2 \dfrac{(x_k - x_s)^{\alpha_2+1}}{\alpha_2+1} + k_3 \dfrac{(x - x_i)^{\alpha_3+1} - (x_k - x_i)^{\alpha_3+1}}{\alpha_3+1}}, & x > x_k. \end{cases} \tag{28}$$

$$k_2 = \frac{\dfrac{(x_s - x_i)^{\alpha_1+1}}{\alpha_1+1}\left[\dfrac{x_s\,(\alpha_1+1) + x_i}{\alpha_1+2} - M(x)\right]}{\begin{array}{r}\dfrac{(x_k - x)^{\alpha_2+1}\,[x\,(\alpha_2+1) + x_k] - (x_k - x_s)^{\alpha_2+1}\,[x_s\,(\alpha_2+1) + x_k]}{(\alpha_2+1)\,(\alpha_2+2)} + \\ -\dfrac{M(x)}{\alpha_2+1}\left[(x_k - x)^{\alpha_2+1} - (x_k - x_s)^{\alpha_2+1}\right]\end{array}}, \quad x_s \le x < x_k \tag{29}$$

$$k_3 = \frac{\begin{array}{r}(x_s - x_i)^{\alpha_1+1}\,\dfrac{x_s\,(\alpha_1+1) + x_i}{(\alpha_1+1)\,(\alpha_1+2)} + k_2\,(x_k - x_s)^{\alpha_2+1}\,\dfrac{x_s\,(\alpha_2+1) + x_k}{(\alpha_2+1)\,(\alpha_2+2)} + \\ -M(x)\left[\dfrac{(x_s - x_i)^{\alpha_1+1}}{\alpha_1+1} + k_2 \dfrac{(x_k - x_s)^{\alpha_2+1}}{\alpha_2+1}\right]\end{array}}{\begin{array}{r}\dfrac{M(x)}{\alpha_3+1}\left[(x - x_i)^{\alpha_3+1} - (x_k - x_i)^{\alpha_3+1}\right] + \\ -\dfrac{(x - x_i)^{\alpha_3+1}\,[x\,(\alpha_3+1) + x_i] - (x_k - x_i)^{\alpha_3+1}\,[x_k\,(\alpha_3+1) + x_i]}{(\alpha_3+1)\,(\alpha_3+2)}\end{array}}, \quad x > x_k \tag{30}$$

$$b = \left\{\frac{(x_s - x_i)^{\alpha_1+1}}{\alpha_1+1} + k_2 \frac{(x_k - x_s)^{\alpha_2+1}}{\alpha_2+1} + \frac{k_3}{\alpha_3+1}\left[(2c)^{\alpha_3+1} + (x_k - x_i)^{\alpha_3+1}\right]\right\}^{-1}. \tag{31}$$

the function $\phi_2(x)$ is increasing inside the interval $x_s \le x < x_k$; therefore, it is represented by $bk_2\,(x_k - x)^{\alpha_2}$. Also, $\phi_2(x_k) \to \infty$ for $\alpha_2 < 0$.

The evaluation of the exponents α_1, α_2, and α_3, is carried out using the methodology previously implemented. To calculate α_1, the reinjection points verifying $x_j < x_s$ are utilized to obtain the corresponding

By means of Eqs. (7) and (27) the function $M(x)$ is shown in Eq (28). The k_2 parameter is obtained using the M_2 function whose numerical values are known (Eq. 29). Similarly, with M_3 and k_2 the k_3 coefficient is calculated (Eq. 30). Finally, the normalization condition is implemented to obtain b, (Eq. 31), where $2c$ is the length of the laminar interval.

Figure 12 shows the numerical data and the theoretical results for functions $M(x)$ and the RPDs for two numerical experiments. It is possible to observe that the RPD are discontinuous functions, and each one of them has two singular points verifying $\phi(x) \to \infty$. Also, the functions $M(x)$ are discontinuous, where its discontinuities coincide with the discontinuities of the corresponding RPD. Finally, note that the analytical results and the numerical data show very good accuracy.

6 Conclusions

In this paper, a study of type-I intermittency with discontinuous RPD functions in one-dimensional maps with quadratic local form was carried out. The methodology employed is an extension of the analytical formulation introduced by del Río and Elaskar [22,23]. The new theoretical methodology implements a more general function $M(x)$ and has proven to be an adequate tool to treat discontinuous RPD for type-I intermittency.

The discontinuous RPD functions are produced by the existence of at least two different reinjection mechanisms. One of them is generated by trajectories passing around the zero derivative point of the quadratic local map; these trajectories produce a high concentration of reinjection points inside of a sub-interval close to the lower limit of the laminar interval. Therefore, the RPD function is discontinuous and it presents a huge density close to the laminar interval lower limit. On the other hand, the characteristic relation, $\langle l \rangle \propto \varepsilon^{-1/2}$, is sustained because the elevated density close to the lower limit of the laminar interval increases the average laminar length without modifying the characteristic relation. Then, the characteristic relation holds although the RPD does not have a monotonically decreasing form as it had been postulated in previous works. This result can be understood because the maximum laminar length verifies the relation $l(-c, c) \propto \varepsilon^{-1/2}$, and the average laminar length, due to the high local concentration, is a fraction of the maximum laminar length.

The extended methodology to evaluate the function $M(x)$ has been implemented to deal with type-I intermittency in the three-wave truncation model for the DNLS equation (DNLS). In this model type-I intermittency with discontinuous RPD appears. The numerical results and the analytical predictions for the nonlinear

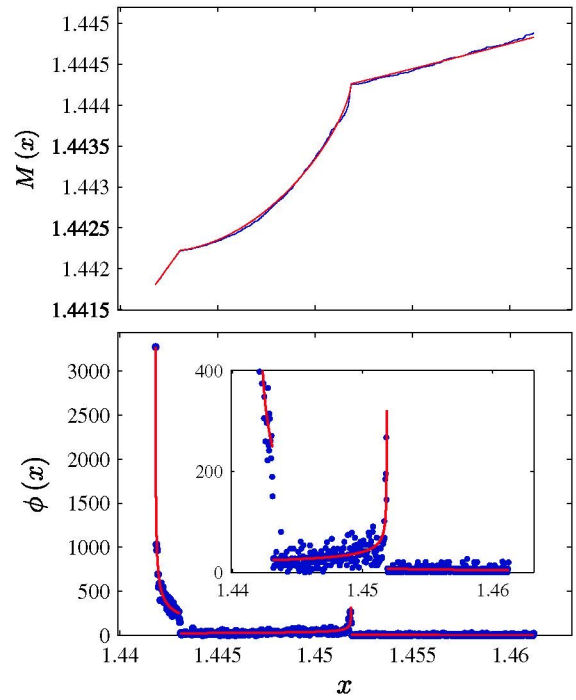

(a) $\varepsilon = 1 \times 10^{-5}$, $c = 0.01$

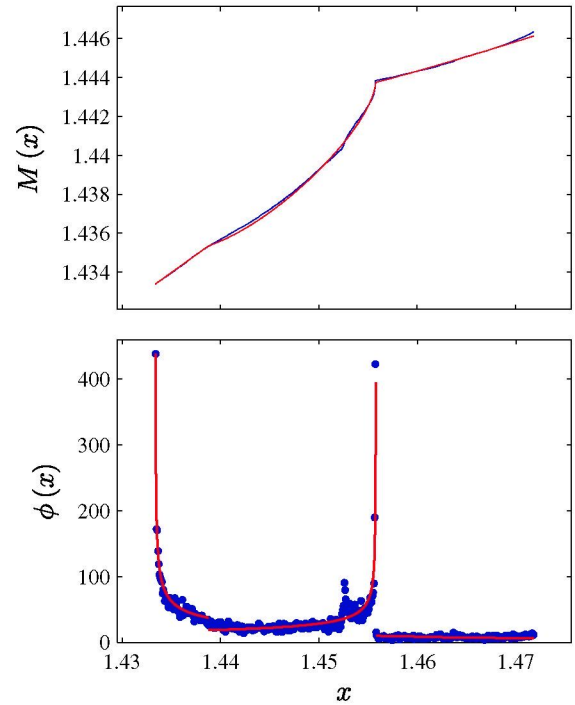

(b) $\varepsilon = 1 \times 10^{-3}$, $c = 0.02$

Fig. 12 Comparison between numerical data and analytical approach of the RPD for the truncated model of the DNLS equation

functions $M(x)$ and for the discontinuous RPD functions present very good accuracy.

Acknowledgments This work has been supported by CONICET (Argentina) under Project PIP 11220090100809, by the Spanish Ministry of Science and Innovation under Project FIS2010-20054, and by Grants of the National University of Córdoba and MCyT of Córdoba, Argentina.

References

1. Manneville, P., Pomeau, Y.: Intermittency and Lorenz model. Phys. Lett. A. **75**, 1–2 (1979)
2. Pomeau, Y., Manneville, P.: Intermittent transition to turbulence in dissipative dynamical system. Commun. Math. Phys. **74**, 189–197 (1980)
3. Nayfeh, A., Balachandran, B.: Applied Nonlinear Dynamics. Wiley, New York (1995)
4. Dubois, M., Rubio, M., Berge, P.: Experimental evidence of intermittencies associated with a subharmonic bifurcation. Phys. Rev. Lett. **16**, 1446–1449 (1983)
5. Malasoma, J., Werny, P., Boiron, M.: Multichannel type-I intermittency in two models of Rayleigh-Bénard convection. Phys. Rev. Lett. **51**, 487–500 (2004)
6. Stavrinides, S., Miliou, A., Laopoulos, T., Anagnostopoulos, A.: The intermittency route to chaos of an electronic digital oscillator. Int. J. Bifurc. Chaos **18**, 1561–1566 (2008)
7. Sanchez-Arriaga, G., Sanmartin, J., Elaskar, S.: Damping models in the truncated derivative nonlinear Schrödinger equation. Phys. Plasmas **14**, 082108 (2007)
8. Pizza, G., Frouzakis, C., Mantzaras, J.: Chaotic dynamics in premixed hydrogen/air channel flow combustion. Combust. Theor. Model. **16**, 275–299 (2012)
9. Nishiura, Y., Ueyama, D., Yanagita, T.: Chaotic pulses for discrete reaction diffusion systems. SIAM J. Appl. Dyn. Syst. **4**, 723–754 (2005)
10. de Anna, P., Le Borgne, T., Dentz, M., Tartakovsky, A., Bolster, D., Davy, P.: Flow intermittency, dispersion and correlated continuous time random walks in porous media. Phys. Rev. Lett. **110**, 184502 (2013)
11. Stan, C., Cristescu, C., Dimitriu, D.: Analysis of the intermittency behavior in a low-temperature discharge plasma by recurrence plot quantification. Phys. Plasmas **17**, 042115 (2010)
12. Chian, A.: Complex System Approach to Economic Dynamics. Lecture Notes in Economics and Mathematical Systems, pp. 39–50. Springer, Berlin (2007)
13. Zebrowski, J., Baranowski, R.: Type I intermittency in nonstationary systems: models and human heart-rate variability. Physica A **336**, 74–86 (2004)
14. Paradisi, P., Allegrini, P., Gemignani, A., Laurino, M., Menicucci, D., Piarulli, A.: Scaling and intermittency of brains events as a manifestation of consciousness. AIP Conf. Proc. **1510**, 151–161 (2012)
15. Schuster, H., Just, W.: Deterministic Chaos. Wiley VCH, Mörlenbach (2005)
16. Kaplan, H.: Return to type-I intermittency. Phys. Rev. Lett. **68**, 553–557 (1992)
17. Price, T., Mullin, P.: An experimental observation of a new type of intermittency. Physica D **48**, 29–52 (1991)
18. Platt, N., Spiegel, E., Tresser, C.: On-off intermittency: a mechanism for bursting. Phys. Rev. Lett. **70**, 279–282 (1993)
19. Kye, W., Rim, S., Kim, C., Lee, J., Ryu, J., Yeom, B., Park, Y.: A new type of intermittent transition to chaos. J. Phys A **16**, L109–L112 (1983)
20. Kim, C., Kwon, O., Lee, E., Lee, H.: New characteristic relation in type-I intermittency. Phys. Rev. Lett. **73**, 525–528 (1994)
21. Hirsch, E., Huberman, B., Scalapino, D.: Theory of intermittency. Phys. Rev. A **25**, 519–532 (1982)
22. del Rio, E., Elaskar, S.: New characteristic relation in type-II intermittency. Int. J. Bifurc. Chaos **20**, 1185–1191 (2010)
23. Elaskar, S., del Rio, E., Donoso, J.: Reinjection probability density in type-III intermittency. Physica A **390**, 2759–2768 (2011)
24. del Rio, E., Sanjuan, M., Elaskar, S.: Effect of noise on the reinjection probability density in intermittency. Commun. Nonlinear Sci. Numer. Simulat. **17**, 3587–3596 (2012)
25. del Rio, E., Elaskar, S., Donoso, J.: Laminar length and characteristic relation in type-I intermittency. Commun. Nonlinear Sci. Numer. Simulat. **19**, 967–976 (2014)
26. del Rio, E., Elaskar, S., Makarov, V.: Theory of intermittency applied to classical pathological cases. Chaos **23**, 033112 (2013)
27. Rogister, A.: Parallel propagation of nonlinear low-frequency waves in high-β plasma. Phys. Fluids **14**, 2733–2739 (1971)
28. Mjolhus, E.: On the modulation instability of hydromagnetic waves parallel to the magnetic field. J. Plasma Phys. **16**, 321–334 (1976)
29. Borotto, F., Chian, A., Hada, T., Rempel, E.: Chaos in driven Alfvén systems: boundary and interior crises. Physica D **194**, 275–282 (2004)